

Accelerating Instanton Theory with the Line Integral String Method, Gaussian Process Regression, and Selective Hessian Modeling

Chenghao Zhang,^{*,†} Amke Nimmrich,[‡] Axel Gomez,[¶] Munira Khalil,[‡] and
Niranjan Govind^{*,†,‡}

[†]*Physical and Computational Sciences Directorate, Pacific Northwest National Laboratory,
Richland, WA 99352, USA*

[‡]*Department of Chemistry, University of Washington, Seattle, WA 98195, USA*

[¶]*Department of Chemistry, Princeton University, Princeton, NJ, 08544, USA*

E-mail: chenghao.zhang@pnnl.gov; niri.govind@pnnl.gov

Abstract

We develop a Gaussian process regression enhanced line integral string method to accelerate ring polymer instanton calculations of tunneling rates and tunneling splittings in molecular proton transfer reactions. By exploiting uncertainty estimates from the surrogate representation, we show that the number of force evaluations required to converge an instanton path becomes effectively independent of the number of beads used to discretize the pathway. To reduce the computational overhead associated with training, particularly when Hessian information is included, we implement graphics processing unit accelerated black box matrix matrix multiplication, achieving an order of magnitude speedups relative to standard implementations. For rate calculations, we introduce a selective Hessian training strategy that distinguishes flexible modes

strongly coupled to the transferring proton from more rigid modes weakly coupled to the reaction coordinate. This enables the construction of accurate surrogate potential energy surfaces with substantially fewer Hessian evaluations. Applications to malonaldehyde and Z-3-aminopropenal demonstrate that tunneling rates can be predicted within 20% of exact values while reducing force and Hessian evaluations. The approach is further extended to tunneling splitting calculations for the formic acid dimer and malonaldehyde, yielding splittings in reasonable agreement with experiment and high level theoretical results.

1 Introduction

Intramolecular proton transfer is a fundamental chemical process that involves coupled electronic and atomic motion. Including nuclear quantum effects, such as quantum tunneling, is crucial for an accurate description of proton transfer through a barrier, even at room temperature. Direct solution of the Schrödinger equation can provide the exact tunneling rate. However, its computational cost scales exponentially with the number of degrees of freedom (DOF), which makes this approach impractical for large molecules. Advanced wave function based methods, including the Multi-Configuration Time-Dependent Hartree (MCTDH) method¹⁻³ and tensor-train methods,^{4,5} have shown promise as practical alternatives. Ring polymer instanton theory⁶⁻¹² provides an efficient way to study tunneling rates in complex molecular systems with sufficient accuracy. In Feynman’s path integral formulation, the instanton represents the path that gives the dominant contribution to the tunneling rate. In instanton theory, the tunneling rate is obtained from a path integral that is approximated by the instanton and the harmonic fluctuations surrounding it. This approach achieves computational efficiency by avoiding explicit sampling of the large number of molecular geometries required in wave function based treatments and enables the inclusion of tunneling effects in atomistic simulations where classical transition state theory fails.

Instanton theory has been an active area of research. A derivation from first principles

has been proposed.^{13,14} Extensions to non-adiabatic systems have been developed,^{15–19} and several studies have introduced corrections to address rate calculation errors near the cross-over temperature.^{20–26} Perturbative corrections up to fourth derivatives of the potential have also been incorporated.^{27,28} In addition, microcanonical rate theory^{29–31} has been formulated within the instanton framework.

On the algorithmic side, the application of ring polymer instanton theory requires locating the instanton path in a high-dimensional quantum system, followed by evaluation of the fluctuation factor through Hessians of the potential at the ring polymer beads. Although instanton theory is more efficient than full-dimensional wave function methods, it remains more computationally demanding than classical transition state theory, especially when combined with on-the-fly electronic structure calculations. This computational cost has limited its broader application to complex molecular systems.

Gaussian Process Regression (GPR) based methods^{32–34} and neural network approaches³⁵ have been developed to accelerate instanton calculations. A chain-of-states approach called the Line Integral Nudged Elastic Band (LI-NEB) method,^{36,37} in the same spirit as the NEB method,^{38,39} has been introduced for instanton path optimization. In our previous work,⁴⁰ we combined LI-NEB with GPR to locate the instanton path and achieved an order of magnitude reduction in the number of force evaluations required. The LI-NEB and string methods have also been implemented for zero-temperature instanton path searches and tunneling splitting calculations.^{41,42}

In this follow-up study to our previous work,⁴⁰ we develop a GPR enhanced Line Integral String (LI-String) method for efficient instanton path optimization. The string method^{43,44} is used to minimize the abbreviated action to obtain the instanton path.^{41,42} We further show that, when using the surrogate model generated by GPR, the cost of converging the instanton path no longer scales with the number of beads representing the path.⁴⁵ Hyperparameter optimization in GPR based on Cholesky decomposition is inefficient, which limits the applicability of GPR to larger systems.^{34,46,47} We demonstrate that the Blackbox Ma-

trix Matrix Multiplication (BBMM) approach and its GPU implementation⁴⁸ can accelerate GPR model training. For intramolecular proton transfer reactions, the selective Hessian training strategy³⁴ further reduces the cost of Hessian evaluations required for computing ring polymer instanton rates. We then apply the GPR enhanced LI-String method to compute the ground state tunneling splitting of two prototypical systems, malonaldehyde and the formic acid dimer (FAD).

The paper is organized as follows. In Section 2, for completeness, we briefly introduce ring polymer instanton theory, the LI-String method, and GPR-based surrogate modeling used for path optimization and rate calculations, including aspects of our implementation. Section 3 focuses on algorithmic acceleration of instanton calculations, including low-scaling path optimization, GPU-accelerated GPR hyperparameter training, and adaptive regression strategies with selective Hessian modeling. In Section 4, we apply the proposed approach to representative intramolecular proton transfer system and finally, we summarize the main conclusions and discuss future directions in Section 5.

2 Theory

2.1 Ring Polymer Instanton Theory

Semiclassical instanton theory provides a practical way to approximate tunneling rates using the optimal tunneling path, which removes the need for explicit path sampling. As a result, the instanton method offers an efficient and tractable approach for computing rates in complex molecular systems. The rate constant is proportional to the imaginary part of the partition function, which is evaluated using Feynman’s path integral formulation in Euclidean space within the steepest descent approximation. The saddle point in the path configuration space corresponds to the instanton path. To evaluate the rate, fluctuations around this path must also be included. Full technical details can be found in previous

works.^{12,49} Here, we summarize the key results and present the instanton rate expression:

$$k_{\text{inst}}(\beta) = A_{\text{inst}}(\beta) e^{-S[\tilde{x}]/\hbar} \quad (1)$$

Here $\beta = 1/(k_B T)$ is the inverse temperature, \tilde{x} is the instanton path, and $A_{\text{inst}}(\beta)$ is the prefactor that accounts for the fluctuation contributions to the rate.

The implementation of the instanton algorithm involves two stages. In the first stage, the instanton path \tilde{x} is located using a path optimization algorithm. In the second stage, the instanton rate k_{inst} is evaluated using Eq. 1. Calculation of the prefactor $A_{\text{inst}}(\beta)$ requires Hessians of the potential energy at all ring polymer beads along the instanton path, and these Hessian evaluations constitute the most computationally intensive part of the calculation.

In this work, we perform the path optimization using the efficient GPR enhanced LI-String method. The cost of the rate calculation is reduced by training the GPR model on data from a small subset of beads and using the model to predict the Hessians of the remaining beads. Training the GPR model with Hessian information can be computationally expensive for large systems and can also be numerically unstable, although this issue is mitigated by the adaptive regression strategy previously introduced.⁴⁰ The selective Hessian strategy provides an additional reduction in cost by limiting explicit Hessian evaluations to a small number of beads. As an alternative, the Hessians of the ring polymer beads can be interpolated using cubic spline interpolation.³⁷ In numerical tests, both cubic spline interpolation and regression perform well in the presence of low noise. When the noise level is high, however, cubic spline interpolation is less robust and can suffer from large approximation errors, as it has to pass exactly through all noisy data points.

2.2 Line Integral String Method

In the Line Integral String (LI-String) method,^{41,42} the instanton path is represented by a string, which is a smooth curve with an intrinsic parameterization. In our approach, the

string is discretized into beads that are maintained at equal arc length spacing. Forces are projected perpendicular to the path to prevent the parallel component from interfering with bead redistribution. Instead of using spring forces to maintain the bead distribution, as in the LI-NEB method, we introduce a reparameterization step whenever the bead spacing becomes uneven. In our implementation, the fast inelastic relaxation engine (FIRE) method^{50,51} provides an efficient optimizer for locating the instanton path. Other optimizers, including quick-min and L-BFGS, can also be used.⁵² Additional details are provided in Appendix A. The LI-String method has also been applied to locate instantons at zero temperature and to compute tunneling splittings.^{41,42}

The constrained dynamics approach^{40,53} is used to compute the path temperature accurately. In addition, GPR can enhance the LI-String method by allowing the path optimization to proceed on a surrogate potential energy surface.

2.3 Gaussian Process Regression

Gaussian Process Regression (GPR) is a machine learning method capable of learning the potential energy surface (PES) of molecules and materials. It has been widely applied to accelerate geometry optimization, transition state searching,^{54,55} and path searching.^{56,57} For the present application, GPR can generate a highly accurate representation of the PES in the vicinity of the instanton path using a relatively small number of training points. Once trained, the GPR model can be used to predict gradients and Hessians at the ring polymer beads, which significantly accelerates the instanton rate calculation. The optimization of the instanton path with GPR is performed iteratively and consists of two steps: optimizing the path on the surrogate PES generated by GPR and then adding new *ab initio* data to update the GPR model. Details of applying GPR to accelerate instanton path searching can be found in the related literature³²⁻³⁴ and in our previous work.⁴⁰

A key advantage of GPR is its ability to provide uncertainty estimates together with its predictions. By incorporating the GPR force uncertainty as the convergence criterion, the

number of required force evaluations becomes independent of the number of beads used to converge the instanton path.⁴⁵ The procedure for computing the force uncertainty estimate is described in Appendix B.

2.3.1 GPR Hyperparameter Optimization

Although GPR can accelerate instanton path optimization and instanton rate calculations, it also introduces non-negligible computational overhead. In particular, the optimization of GPR hyperparameters is computationally inefficient, and this bottleneck becomes more severe when Hessians are included in the GPR model. To address this challenge, we use the Blackbox Matrix Matrix Multiplication (BBMM) approach implemented in GPyTorch and employ GPU hardware to accelerate GPR model optimization.⁵⁸ The BBMM method reduces the cost of exact Gaussian process inference from $O(n^3)$ to $O(n^2)$. In BBMM, the optimization of GPR hyperparameters relies solely on matrix vector multiplications, which can be efficiently accelerated using parallel computing and GPUs. We briefly review the method here and refer the reader to Ref. 58 for complete details.

The performance of the GPR model depends on a set of hyperparameters θ , which include likelihood noise and kernel lengthscales l_d . During model training, these hyperparameters are optimized by minimizing the negative log marginal likelihood,

$$L(\theta|X, y) = -\log p(\theta|X, y) = \frac{1}{2}y^T K_{XX}^{-1}y + \frac{1}{2} \log(|K_{XX}|) + \frac{n}{2} \log(2\pi). \quad (2)$$

In the conventional approach, Cholesky decomposition is used to compute $K_{XX}^{-1}y$ and the log determinant $\log(|K_{XX}|)$. The $O(n^3)$ cost of the Cholesky decomposition makes this approach inefficient for large training sets. In the BBMM method, the linear conjugate gradient algorithm⁵⁹ is used to solve $K_{XX}^{-1}y$, and the trace estimator^{60,61} is used to approximate $\log(|K_{XX}|)$. The algorithm integrates the Lanczos tridiagonalization procedure required for log determinant evaluation with the conjugate gradient iterations and employs a precondi-

tioner to accelerate convergence.

In practice, the conjugate gradient method converges in p iterations and has computational cost $O(pn^2)$ with $p \ll n$. The Hutchinson trace estimator⁶⁰ approximates $\log(|K_{XX}|)$ using t random vectors with computational cost $O(tn^2)$, where $t \ll n$. Together, these ingredients reduce the overall time complexity of GP inference to $O(n^2)$, which is more efficient than the $O(n^3)$ cost associated with the Cholesky decomposition.

3 Algorithmic Acceleration of Instanton Calculations

3.1 Low-Scaling Line Integral String Algorithm

By utilizing force uncertainty estimates from the GPR model, the number of force evaluations required to converge the path has been shown to be independent of the number of beads in the NEB method.⁴⁵ This allows the selection of the optimal number of beads to represent the path at no additional cost. In this section, we show that a similar advantage extends to the GPR-enhanced LI-String method.

In complex molecular systems, a large number of beads are typically required to represent the path with reasonable accuracy. In the conventional instanton path searching algorithm, this is achieved by starting the path search with a small number of beads and then increasing the bead number through path interpolation followed by further path optimization. In general, increasing the number of beads leads to a larger number of required force evaluations. In contrast, by using force uncertainty estimates from the GPR model, we show in Fig. 1 that the number of force evaluations is independent of the number of beads used to represent the path in the LI-String method.

We demonstrate the advantage of the GPR-LI-String method by comparing its performance with the conventional Hessian-based instanton optimization algorithm, the Quasi-Newton (QN) method.⁵⁹ In the Quasi-Newton method, we first locate the instanton path using $N = 20$ beads and then further optimize the path by increasing the number of beads

to achieve higher accuracy. Cubic spline interpolation is used to determine the starting geometries of the new ring polymer beads. The ring polymer Hessian expansion approach⁶² is employed to interpolate Hessians at the locations of the new beads, which eliminates the need for additional Hessian calculations. However, additional force evaluations are still required to optimize the path.

In Fig. 1(a), we compare the performance of the GPR-LI-String and QN methods for malonaldehyde at $T = 250$ K. Using the QN method, 280 force evaluations are required to find the instanton path with $N = 20$ beads, with an additional 120 and 240 force evaluations needed to further optimize the path with $N = 40$ and $N = 80$ beads, respectively. In contrast, using the GPR-enhanced LI-String method, 64 force evaluations are required to locate the instanton path with $N = 10$ beads, and increasing the number of beads to $N = 80$ requires only 8 additional force evaluations. This demonstrates favorable scaling of the computational cost with respect to the number of beads.

In Fig. 1(b), we perform the benchmark test for aminopropenal at $T = 250$ K. Using the QN method, 240 force evaluations are required to locate the instanton path with $N = 20$ beads, with an additional 120 and 320 force evaluations needed to further optimize the path with $N = 40$ and $N = 80$ beads, respectively. In contrast, using the GPR-enhanced LI-String method, 70 force evaluations are required to locate the instanton path with $N = 10$ beads. Increasing the number of beads from $N = 10$ to $N = 80$ requires only 10 additional force evaluations.

3.2 GPU-Accelerated GPR Hyperparameter Training

To demonstrate the improved performance of the GPU-accelerated BBMM method for training the GPR model, we benchmark it against BBMM on CPU and GPU, the Cholesky method on CPU and GPU, and the pseudo-inverse (PI) method on CPU using two example molecules: malonaldehyde and Z-3-aminopropenal. For the Cholesky algorithm, we use the implementation provided in GPyTorch. For the pseudo-inverse method, we use the `pinv()`

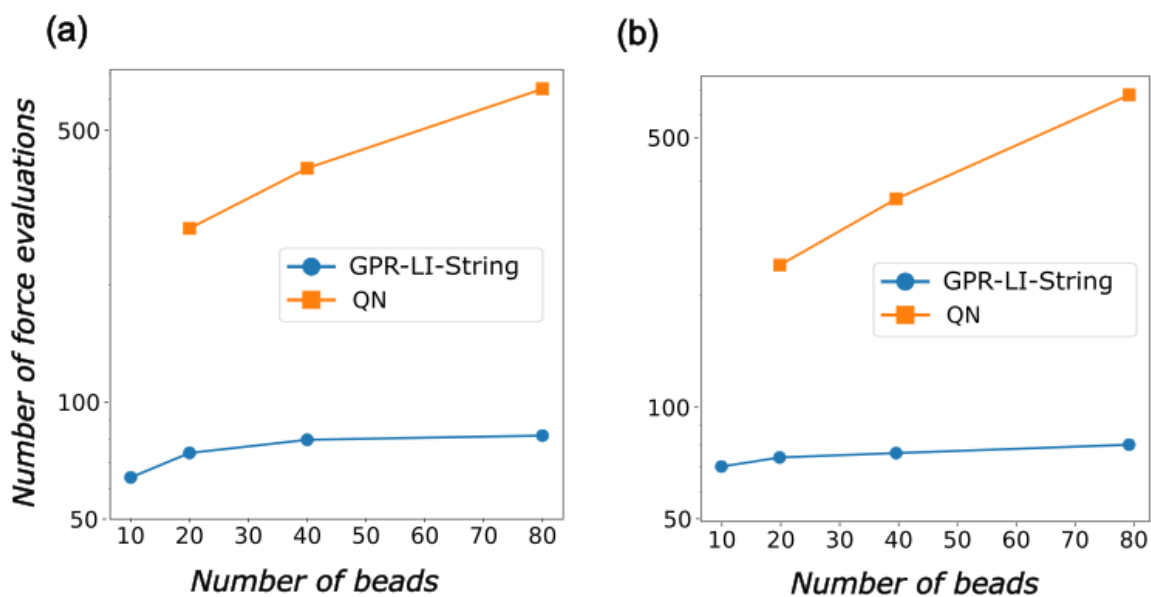


Figure 1: Comparison of the number of force evaluations required to achieve convergence as a function of the number of beads for the Quasi-Newton (QN) method and the GPR-enhanced LI-String method (GPR-LI-String). (a) Malonaldehyde instanton path at $T = 250$ K. (b) Aminopropenal instanton path at $T = 250$ K.

and `logdet()` functions implemented in PyTorch and supported by LAPACK. The training data for malonaldehyde include 20 potential and gradient data points and 10 Hessian data points. Among the 21 internal modes, 13 modes are included in the GPR model, and the rest 8 modes are treated by the linear regression. The training data for Z-3-aminopropenal include 80 potential and gradient data points and 20 Hessian data points. Among the 24 internal modes, 12 modes are included in the GPR model, and the rest 12 modes are treated by the linear regression.

The GPR model training times are shown in Fig. 2. Both the GPU-accelerated BBMM method and the GPU-accelerated Cholesky method are efficient for GPR training. For the two example molecules, GPR model training on GPU is completed within a few minutes. Although the theoretical time complexity of the BBMM method is lower than that of the Cholesky algorithm, this advantage is not significant for the test cases studied here. Compared to the GPR model trained with the BBMM method on CPU, the GPU implementation is an order of magnitude faster for the molecular systems we have considered, demonstrating the suitability of the BBMM method for GPU acceleration.

The PI method on CPU shows performance comparable to that of the BBMM method on CPU. However, in these numerical tests, we do not observe a performance gain when the PI algorithm is executed on GPU. The Cholesky method on CPU is the most computationally inefficient implementation among all methods tested. Notably, in our tests, the Cholesky method exhibits a larger performance improvement upon GPU acceleration than the BBMM method.

3.3 Adaptive Regression, Selective Hessian Training, and Hessian Interpolation

In this section, we demonstrate the performance of selective Hessian training for intramolecular proton transfer systems. The internal coordinates form a high-dimensional space, in which the instanton path spans a subspace that we refer to as the active subspace. Its or-

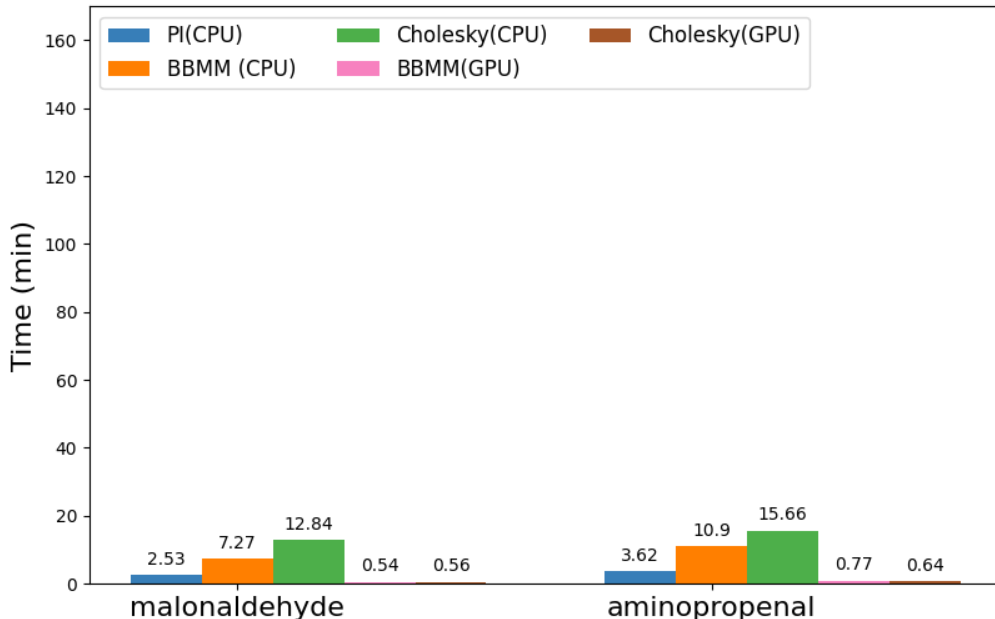


Figure 2: GPR hyperparameter training time for three different molecules using the pseudo-inverse method (PI, blue), BBMM on CPU (orange), Cholesky decomposition on CPU (green), BBMM on GPU (pink), and Cholesky decomposition on GPU (brown), reported in minutes. Details of the training datasets are provided in the text. NEED to update this plot for the arxiv submission.

thogonal complement is the null subspace. Examining how each internal mode contributes to the tangent direction of the path reveals which modes form the active subspace and which belong to the null subspace. In proton transfer reactions, the active subspace consists of internal coordinates that are strongly coupled to the transferring proton and are referred to as flexible internal modes. The null subspace comprises coordinates that are weakly coupled to the proton, which we term rigid internal modes.

The rigid modes, which lie in the null subspace, act as irrelevant input variables in the GPR model. Inclusion of these modes can lead to unstable hyperparameter optimization, increased computational cost, and poor model generalization. To address this challenge, we employ an adaptive regression strategy.⁴⁰ The gradients and Hessians of the potential $V(x)$ in the active subspace are modeled using GPR, while those in the null subspace are modeled using linear regression.

The partial Hessians in the null subspace are modeled using a linear regression approach,

which requires fewer beads for accurate representation. In contrast, the active subspace employs a more expressive GPR model and therefore requires a larger number of beads to achieve accurate modeling. The selective Hessian training approach,³⁴ applied separately to the active and null subspaces, leads to substantial reductions in computational cost. We illustrate this approach using ground-state proton transfer in malonaldehyde, Z-3-aminopropenal.

The rigorous instanton rate is computed using a potential energy surface generated on the fly with density functional theory (DFT). The instanton rate calculation can be accelerated by using the surrogate energy surface obtained from the adaptive regression strategy. In addition, cubic spline interpolation can be used to approximate Hessians at the ring polymer beads. For all cases presented below, we benchmark the rigorous instanton rate against the approximate rate. For the approximate rate calculations, we consider three cases that differ in the construction of the training data and the method used to approximate Hessians: (a) full Hessians are computed at selected beads for GPR modeling, (b) partial Hessians in the null subspace are computed at three beads and partial Hessians in the active subspace are computed at selected beads for GPR modeling, and (c) full Hessians are computed at selected beads for cubic spline interpolation.

4 Results

4.1 Ground-State Proton Transfer Rates

4.1.1 Malonaldehyde

In Table 1, we report the instanton rate constant k for ground-state intramolecular proton transfer in malonaldehyde at two temperatures, $T = 275$ K and $T = 200$ K. At the higher temperature, $T = 275$ K, using 10 full Hessian training data points in the model allows prediction of the instanton rate with less than 20% error. If we use 3 partial Hessian data points along 13 rigid modes and 10 partial Hessian data points along 8 flexible modes as

training data, the approximate instanton rate remains accurate, with an error of about 6%. This approach reduces the number of force evaluations by 44% compared to using the full Hessian dataset. The Hessians of the ring polymer beads can also be approximated using cubic spline interpolation with 20 Hessian data points spaced equally along the instanton path, yielding an approximate instanton rate with less than 20% error.

The potentials $V(q)$, gradients $\nabla V(q)$ and Hessians $\nabla^2 V(q)$ are modeled via regression as $y = \epsilon + f(q)$, where ϵ denotes the noise and $f(q)$ is the function learned by GPR. We show that the accuracy of GPR predicted tunneling rates can be enhanced by increasing the accuracy of the underlying DFT calculations, which effectively reduces ϵ . Numerically, this is accomplished by tightening the convergence threshold for the electron density and the DFT integration grid. At $T = 275\text{K}$, we report that using a tight DFT convergence criterion together with a fine DFT grid, and 10 full Hessian training data points in the model enables prediction of the instanton rate within 6 % error, representing an improvement in accuracy relative to the standard DFT convergence test case.

At the lower temperature, $T = 200\text{ K}$, accurately predicting the instanton rate using the surrogate energy surface requires more training data. We find that using 3 partial Hessian data points along 13 rigid modes and 20 partial Hessian data points along 8 flexible modes as training data allows the instanton rate to be approximated within 10% error relative to the rigorous instanton rate. This approach reduces the number of force evaluations by 52% compared to using the full Hessian dataset. The Hessians of the ring polymer beads can also be approximated using cubic spline interpolation, resulting in an approximate rate with an error of less than 5%.

4.1.2 Z-3-aminopropenal

In Table 2, we report the instanton rate constant k for ground-state intramolecular proton transfer in Z-3-aminopropenal at two temperatures, $T = 250\text{ K}$ and $T = 160\text{ K}$. At $T = 250\text{ K}$, using 3 partial Hessian training data points along rigid modes and 20 partial Hessian

Table 1: Ground state intramolecular proton transfer in malonaldehyde. Comparison of the instanton rate computed (a) on a surrogate potential energy surface, where Hessians in the active subspace are fitted using GPR, employing the same number of beads as used for the null subspace, which is modeled with linear regression. (b) On a surrogate potential energy surface, where Hessians in the null subspace are fitted with only 3 beads. (c) Hessians are fitted with cubic spline interpolation. (d) Potential energy surface computed using DFT. For malonaldehyde, there are 21 internal modes.

T(K)	DFT convergence	Training set	bead number N	rate constant (ps^{-1})	error (%)
275	standard	(a) 20V, 20 G, 10 H	40	7.86	20.7
			320	8.07	18.7
		(b) 20V, 20 G	40	6.12	6.0
		10 H (8 flexible), 3 H (13 rigid)	320	7.25	6.6
		(c) 20 H (cubic spline)	40	5.35	17.8
			320	5.62	17.3
	tight	(d) DFT	40	6.51	
			320	6.80	
		(a) 20V, 20G, 10H	40	6.50	2.0
			320	6.88	6.3
		(b) 20V, 20G	40	7.75	21.6
		10 H (8 flexible), 3 H (13 rigid)	320	7.99	8.9
200	standard	(c) 20 H (cubic spline)	40	7.83	22.9
			320	8.15	11.0
		(d) DFT	40	6.37	
			320	7.34	
		(a) 50V, 50 G, 20 H	40	4.14	16.3
			320	4.19	6.6
200	standard	(b) 50V, 50 G, 20 H	40	3.29	7.5
		(8 flexible), 3 H (13 rigid)	320	4.10	4.3
		(c) 20 H (cubic spline)	40	3.58	0.6
			320	4.02	2.3
		(d) DFT	40	3.56	
			320	3.93	

training data points along flexible modes, the instanton rate predicted on the surrogate surface is within 20% error relative to the rigorous rate. Along the instanton path at $T = 250$ K, there are 6 flexible modes and 18 rigid modes. This approach reduces the number of force evaluations by 62.5% compared to using the full Hessian dataset. However, we find that the approximate instanton rate calculated with Hessians interpolated by cubic spline interpolation deviates by about 60% from the rigorous rate, which indicates the cubic spline interpolation is less robust in the presence of high noise. We also observe that employing a tight DFT convergence together with a fine integration grid yields the instanton rate predictions with an error within 5% error, which shows an improvement over 20 % error obtained with the standard DFT convergence settings. At the lower temperature, $T = 160$ K, the instanton rate predicted using partial Hessian data has less than 20% error relative to the rigorous rate. Along the instanton path at $T = 160$ K, there are 12 flexible modes and 12 rigid modes. This approach reduces the number of force evaluations by 42% compared to using the full Hessian dataset. The approximate rate can also be calculated with Hessians interpolated by cubic spline interpolation, and we find that the error in the rate is around 20%. Notably, the error rate associated with cubic spline interpolation is observed to increase with temperature. At higher temperature, the instanton path shortens near the barrier top, resulting in densely clustered interpolation points and increased susceptibility of the cubic spline to noise.

4.2 Tunneling Splitting Calculations

The ring polymer instanton method has been developed to compute tunneling splittings with good accuracy.^{63–65} Here, we use the LI-String method accelerated by GPR to compute tunneling splittings for two model systems: formic acid dimer (FAD) and malonaldehyde.

Table 2: Ground state intramolecular proton transfer in Z3-aminopropenal. Comparison of the instanton rate computed (a) on a surrogate potential energy surface, where Hessians in the active subspace are fitted using GPR, employing the same number of beads as used for the null subspace, which is modeled with linear regression. (b) On a surrogate potential energy surface, where Hessians in the null subspace are fitted with only 3 beads. (c) With Hessians fitted with cubic spline interpolation. (d) Potential energy surface computed using DFT. For aminopropenal, there are 24 internal modes.

T(K)	DFT convergence	Training set	bead number N	rate (ps^{-1})	error (%)
250	standard	(a) 80V, 80 G, 20 H	40	122.0	18.4
			320	124.5	19.8
		(b) 80 V, 80 G 20 H (6 flexible), 3 H (18 rigid)	40	120.0	19.1
			320	124.3	20.0
		(c) 20 H (cubic spline)	40	53.8	63.9
			320	65.1	58.1
		(d)DFT	40	148.4	
			320	155.4	
	tight	(a) 80V, 80G, 20 H	40	122.6	16.1
			320	143.8	3.4
		(b) 80 V, 80 G 20 H (6 flexible), 3 H (18 rigid)	40	139.5	4.6
			320	137.6	7.8
(c) 20 H (cubic spline)		40	57.9	60.4	
		320	59.2	60.3	
(d) DFT		40	146.3		
		320	149.2		
160	standard	(a) 80 V, 80 G, 20 H	40	99.8	9.7
			320	112.0	6.1
		(b) 80 V, 80 G 20 H (12 flexible) , 3 H (12 rigid)	40	110.7	21.6
			320	123.5	17.1
		(c) 20 H (cubic spline)	40	75.7	16.8
			320	86.9	17.6
		(d) DFT	40	91.0	
			320	105.5	

4.2.1 Formic Acid Dimer

The ring polymer instanton method has been applied by Richardson to calculate the tunneling splitting of the formic acid dimer (FAD)⁶⁶ on the fitted potential developed by Qu and Bowman,⁶⁷ which shows good agreement with the experimental results.^{68,69}

The ground state potential energy surface of FAD is computed using DFT with the wB97X functional together with the def2-TZVPP basis set. This choice of electronic functional and basis set minimizes the error from the electronic treatment.⁷⁰ The barrier for the double proton transfer is calculated to be 2868 cm⁻¹, which agrees well with the barrier (2853 cm⁻¹) calculated at the CCSD(T)-F12a/haTZ level of theory reported in Ref. 67. In our calculation, the two end beads are fixed at the two symmetric potential minima of the FAD, apart from rotation and translation. During path optimization, the two end beads are reoriented to minimize the Euclidean distance in mass-scaled Cartesian coordinates as described in Ref. 41 using the quaternion method.⁷¹

To speed up the calculation, the path is first optimized using a low-cost PBE0 DFT functional and the 6-31G* basis set. The starting geometry of our LI-String optimization is the minimum energy path obtained using the NEB method. After the instanton path converges with the cheaper method, we switch to the more accurate wB97X functional with the def2-TZVPP basis set to further refine the instanton path optimization. In our calculation, we find that the instanton path can be well represented with 20 beads using the LI-String method. The GPR-accelerated LI-String method is able to find the instanton path with 43 *ab initio* potential and force evaluations using the PBE0 exchange correlation functional and the 6-31G* basis set. The path is further refined with 69 *ab initio* potential and force evaluations using the wB97X exchange correlation functional and the def2-TZVPP basis set.

The force near the reactant and product minima is close to zero, and the GPR model fails to predict accurate forces near the two potential minima. Instead, we fit the force near the two minima using the potential Hessians: $f(x) = -V''(x_0)(x - x_0) + f(x_0)$, when

$|f(x)| < f_c$ and $V(x) - V_{\min} < V_c$. In our calculation, we set $f_c = 1e^{-3}$ a.u. and $V_c = 0.01$ eV. The temperature of the converged instanton path can be computed using the constrained dynamics approach on the fitted potential. In our calculation, we find that the temperature of the optimized path is 7.8 K, which corresponds to $\beta\hbar = 40483$ in atomic units. The Hessians of the ring polymer beads are fitted using cubic spline interpolation with 40 Hessians computed with DFT for beads spaced equally along the path.

In our current implementation, we use the Z-matrix descriptor to construct the GPR model. Unfortunately, the Z-matrix descriptor is not invariant under permutation of atom indices. This drawback can lead to slight asymmetry of the surrogate PES on the two sides of the barrier. To address this issue, the tunneling splitting calculation is performed by employing the instanton bead geometries and potential Hessians defined on one side of the barrier, while the corresponding geometries and Hessians on the opposite side are obtained via a symmetry operation. This issue can also be resolved using descriptors that are invariant to permutations of atom indices, for example, the Atom-Centered Symmetry Functional (ACSF)⁷² or Smooth Overlap of Atomic Positions (SOAP).⁷³

The instanton tunneling splitting is computed using Eq. (29) in Ref. 64 and found to be 0.008 cm^{-1} . This result is in good agreement with the ring polymer instanton calculation in Ref. 66 using the fitted potential⁶⁷ (0.014 cm^{-1}) and quantum dynamics calculation using a neural network potential energy surface (0.0128 cm^{-1}).⁷⁴ Experimentally, the ground state tunneling splitting of FAD has been determined with progressively higher precision, reported as 0.0158 cm^{-1} in 2007,^{68,69} and later refined to be 0.01137 cm^{-1} ⁷⁵ and 0.01117 cm^{-1} ⁷⁶ in more recent measurements. Note that the CCSD(T) method is used to fit the potential energy surface developed by Qu and Bowman,⁶⁷ while we use DFT in our calculation. In Ref. 66, the action S , fluctuation factor Φ , and tunneling splitting Δ using the fitted potential⁶⁷ are reported as $S/\hbar = 14.87$, $\Phi = 17.1$, and $\Delta = 0.014 \text{ cm}^{-1}$. In Table 3, we report our results using a PES learned with GPR at the DFT level of theory. In the SI, we report the harmonic wavenumbers of the minimum and saddle point of FAD from the DFT calculations,

in comparison to the fitted PES.

Table 3: Tunneling splitting Δ in cm^{-1} , action S_{kink}/\hbar , and fluctuation factor Φ for formic acid dimer.

bead number N	Φ	S_{kink}/\hbar	$\Delta(\text{cm}^{-1})$
320	74.72	12.90	0.021
640	78.98	13.52	0.011
1280	77.31	13.84	0.008

4.2.2 Malonaldehyde

For malonaldehyde, the experimentally determined tunneling splitting is 21.583 cm^{-1} .^{77,78} The tunneling splitting of malonaldehyde has been computed using the instanton method^{63,64} on the full-dimensional fitted potential energy surface of Sewell *et al.*,⁷⁹ yielding 57.7 cm^{-1} . The LI-String method and the quadratic LI-String method have also been developed to locate the instanton path at zero temperature and compute the tunneling splitting of malonaldehyde on the same fitted potential,^{41,42} reducing the number of potential energy calls by two orders of magnitude. Furthermore, by combining the ring polymer instanton approach with transfer learning of the PES, the tunneling splitting of malonaldehyde was accurately determined as 25.3 cm^{-1} .⁸⁰

Here, the ground state potential energy surface of malonaldehyde is computed using DFT. We tested two different functional and basis set combinations: (1) the B3LYP exchange correlation functional with the 6-31G* basis set and (2) the B3LYP exchange correlation functional with the def2-TZVPP basis set, both with DFT-D3 dispersion correction. The barriers computed using the B3LYP functional are 3.480 kcal/mol (6-31G* basis set) and 3.317 kcal/mol (def2-TZVPP basis set), which show slight deviation from the barrier (3.8948 kcal/mol) from CCSD(T)/aug-cc-PVTZ calculations reported in Ref. 80. Two end beads are fixed at the reactant and product states and reoriented to minimize the Euclidean distance of the path in mass-scaled Cartesian coordinates.⁴¹ The starting geometry for LI-String optimization is the minimum energy path obtained from the NEB method. The GPR-

accelerated LI-String method is able to locate the instanton path with 118 *ab initio* potential and force evaluations. The forces near the two potential minima are fitted using Hessians at the two minima for improved accuracy. The temperature of the instanton path is computed using the constrained dynamics approach. In our calculation, the temperature is found to be 13 K, corresponding to $\beta\hbar = 24300$ in atomic units. The Hessians of the ring polymers are fitted using cubic spline interpolation with 40 Hessians computed *ab initio* for beads spaced equally along the path. The same symmetry operation described above is applied to the bead geometries and potential Hessians for the tunneling splitting calculation.

The instanton tunneling splitting is found to be 34.34 cm^{-1} using B3LYP/6-31G* and 61.43 cm^{-1} using B3LYP/def2-TZVPP. In Table 1 of Ref. 80, the action S , fluctuation factor Φ , and tunneling splitting Δ computed using the transfer learning PES with the extended dataset are reported as $S/\hbar = 5.743$, $\Phi = 53.2$, and $\Delta = 25.3 \text{ cm}^{-1}$. In Table 4, we report our results using a PES learned with GPR at the DFT level of theory. We find that the DFT treatment slightly underestimates the action of the instanton path compared to the result obtained with the CCSD(T)-level corrected PES, which leads to a larger splitting than that obtained using higher-level electronic structure theory. Despite this, our calculated tunneling splittings show reasonable agreement with the experimental results^{77,78} and the theoretical result using an accurately fitted PES.⁸⁰

Table 4: Tunneling splitting Δ in cm^{-1} , action S_{kink}/\hbar , and fluctuation factor Φ for malonaldehyde.

DFT functional	bead number N	Φ	S_{kink}/\hbar	$\Delta(\text{cm}^{-1})$
b3lyp+6-31g*	320	49.8	5.11	48.01
	640	55.0	5.26	37.86
	1280	56.6	5.34	34.34
b3lyp+ Def2-TZVPP	320	32.84	5.25	64.06
	640	29.51	5.38	63.42
	1280	28.60	5.45	61.43

5 Conclusions

In this work, we developed a GPR-enhanced Line Integral String (LI-String) method to accelerate ring polymer instanton calculations. By leveraging the uncertainty quantification provided by GPR, we show that the number of beads used to represent the instanton path no longer determines the number of force evaluations required for convergence.⁴⁵ A drawback of the traditional GPR implementation is that the computational overhead associated with model training is not negligible, which limits applicability to larger systems, especially when Hessians are included in the training data. Conventional GPR training is inefficient and exhibits unfavorable cubic scaling with the number of training data points, $\sim \mathcal{O}(N^3)$. Here, we apply the Blackbox Matrix Matrix Multiplication (BBMM) method in GPyTorch⁵⁸ and use GPU acceleration to speed up model training. This provides an order-of-magnitude speedup in GPR inference.

Once the instanton path is optimized, the remaining cost of the instanton rate calculation is still approximately n times that of transition state theory, where n is the number of ring polymer beads for which Hessians are required. The GPR model can construct a surrogate energy surface using a relatively small number of Hessian data points and still yield accurate instanton rates, thereby substantially reducing the cost of Hessian evaluations. For proton transfer reactions, we further suggest that Hessian costs can be reduced by combining selective Hessian training³⁴ with the adaptive regression strategy. This is enabled by evaluating Hessian components along rigid modes using fewer beads than are needed for the flexible modes. We illustrate this idea for malonaldehyde and Z-3-aminopropenal, where Hessians along the rigid modes are evaluated using 3 beads and Hessians along the flexible modes are evaluated using 20 beads. The predicted instanton rates remain within 20% of the rigorous instanton rates, with an additional reduction in computational cost ranging from 40% to 62.5%.

Finally, we combine GPR with the LI-String method to accelerate tunneling splitting calculations within the ring polymer instanton framework. Using two prototypical systems,

malonaldehyde and the formic acid dimer, we show that the instanton path can be located with on the order of 100 potential energy and force evaluations. The computed tunneling splittings are in reasonable agreement with experimental measurements and with previous calculations based on fitted potentials or neural network potentials. The remaining discrepancies can be attributed primarily to errors in the underlying potential energy surface. We expect that the developments presented here will find broad application in accelerating tunneling rate and tunneling splitting calculations using ring polymer instanton theory.

Appendices

A Line Integral String Optimization

The objective function for the LI-String method is the abbreviated action $W(\mathbf{r})$:

$$W(\mathbf{r}) = \frac{1}{\hbar} \int_{\mathbf{r}_1}^{\mathbf{r}_n} \sqrt{2(V(\mathbf{r}) - E)} dr, \tag{3}$$

where \mathbf{r}_1 and \mathbf{r}_n are the turning points.

Using mass-scaled Cartesian coordinates, the action $W(\mathbf{r})$ is discretized using n beads:

$$W(\mathbf{r}) \approx \frac{1}{2\hbar} \sum_{j=1}^n \left(\sqrt{2(V(\mathbf{r}_j) - E)} + \sqrt{2(V(\mathbf{r}_{j-1}) - E)} \right) |\mathbf{r}_j - \mathbf{r}_{j-1}|. \tag{4}$$

The LI-String optimization is performed with constraints. The interior beads are maintained at equal arc length spacing, and the two end beads are constrained to move on the energy contour $V(\mathbf{r}) = E$.

Using Lagrange multipliers, we formulate the constrained objective function as

$$L(\mathbf{r}_1, \mathbf{r}_2, \dots, \mathbf{r}_n) = W(\mathbf{r}_1, \mathbf{r}_2, \dots, \mathbf{r}_n) - \lambda_1 (V(\mathbf{r}_1) - E) - \lambda_2 (V(\mathbf{r}_n) - E) \tag{5}$$

where λ_1, λ_2 are Lagrange multipliers associated with the constraints on the two end beads respectively.

The optimization force $\mathbf{g}_j = -\nabla_j W$ is given in Ref. 37. The LI-String method uses projection and reparameterization to efficiently impose the equal arc length constraint $r \hat{\mathbf{t}}$ for the interior beads. The optimization force for bead j includes only the transverse component of \mathbf{g}_j :

$$\mathbf{g}_j^{\text{opt}} = \mathbf{g}_j^\perp. \quad (6)$$

A reparameterization is performed when the bead distribution becomes uneven to re-enforce the constraint. The criterion used for repositioning the beads is

$$\max_i \left| \left| |\mathbf{x}_{i+1} - \mathbf{x}_i| - |\mathbf{x}_i - \mathbf{x}_{i-1}| \right| \right| > \frac{\sum_i |\mathbf{x}_{i+1} - \mathbf{x}_i|}{10(n-1)}. \quad (7)$$

We use cubic spline interpolation of the path to reposition the beads so that they are equally spaced along the curve.

From the Lagrangian formulation in Eq. 5, the converged path satisfies constraints on the potential gradients and energies of the two end beads:

$$\begin{aligned} \sqrt{2\mu(V(\mathbf{r}_2) - E)} \frac{\mathbf{r}_1 - \mathbf{r}_2}{|\mathbf{r}_1 - \mathbf{r}_2|} &= \lambda_1 \nabla V(\mathbf{r}_1), \\ \sqrt{2\mu(V(\mathbf{r}_{n-1}) - E)} \frac{\mathbf{r}_{n-1} - \mathbf{r}_n}{|\mathbf{r}_{n-1} - \mathbf{r}_n|} &= \lambda_2 \nabla V(\mathbf{r}_n), \end{aligned} \quad (8)$$

and

$$\begin{aligned} V(\mathbf{r}_1) &= E, \\ V(\mathbf{r}_n) &= E. \end{aligned} \quad (9)$$

Two energy-constraint terms are introduced to constrain the end beads to the energy contour. In addition, two auxiliary force terms $\mathbf{g}_1^{\text{aux}}$ and $\mathbf{g}_n^{\text{aux}}$ are introduced, with magnitudes

comparable to \mathbf{g}_j^\perp , to facilitate rapid convergence:⁸¹

$$\begin{aligned}\mathbf{g}_1^{\text{aux}} &= \langle |\mathbf{g}_j^\perp| \rangle \frac{\mathbf{r}_2 - \mathbf{r}_1}{|\mathbf{r}_1 - \mathbf{r}_2|}, \\ \mathbf{g}_n^{\text{aux}} &= \langle |\mathbf{g}_j^\perp| \rangle \frac{\mathbf{r}_{n-1} - \mathbf{r}_n}{|\mathbf{r}_{n-1} - \mathbf{r}_n|}.\end{aligned}\tag{10}$$

The final optimization force for the two end beads is

$$\mathbf{g}_{1,n}^{\text{opt}} = \mathbf{g}_{1,n}^{\text{aux}} - \left(\mathbf{g}_{1,n}^{\text{aux}} \cdot \hat{\mathbf{f}}(\mathbf{r}_{1,n}) \right) \hat{\mathbf{f}}(\mathbf{r}_{1,n}) + \kappa (V(\mathbf{r}_{1,n}) - E) \hat{\mathbf{f}}(\mathbf{r}_{1,n}),\tag{11}$$

where the first two terms enforce the potential-gradient constraint in Eq. 8, and the third term enforces the energy constraint in Eq. 9.

The LI-String algorithm is considered converged when

$$|\mathbf{g}_j^{\text{opt}}| < \epsilon^{\text{interior}}, \quad |\mathbf{g}_{1,n}^{\text{opt}}| < \epsilon^{\text{end}}, \quad \sum_{j=2}^{n-1} |\mathbf{g}_j^\perp| < \epsilon^{\text{sum}}.\tag{12}$$

At convergence, we use constrained dynamics^{40,53} to define the temperature as $T = \frac{\hbar}{k_B \tau}$, where k_B is the Boltzmann constant and τ is the oscillation period. This approach provides an accurate temperature estimate, particularly when the instanton path exhibits significant curvature at low temperatures.

B Force Uncertainty Estimation in Gaussian Process Regression

To incorporate derivative information in GPR, the observable vector \mathbf{y} is extended as

$$\mathbf{y}_{\text{ext}} = \left[y^{(1)} \dots y^{(N)}, \frac{\partial y^{(1)}}{\partial q_1^{(1)}} \dots \frac{\partial y^{(N)}}{\partial q_1^{(N)}}, \frac{\partial y^{(1)}}{\partial q_2^{(1)}} \dots \frac{\partial y^{(N)}}{\partial q_2^{(N)}}, \dots, \frac{\partial y^{(1)}}{\partial q_D^{(1)}} \dots \frac{\partial y^{(N)}}{\partial q_D^{(N)}} \right]^\top.\tag{13}$$

where N is the number of training data points and D is the dimension. The covariance matrix $K(Q, Q)$ is extended to include covariance terms between partial derivatives and between the function values and partial derivatives:

$$\mathbf{K}_{\text{ext}} = \begin{bmatrix} K(\mathbf{Q}, \mathbf{Q}) & \frac{\partial K(\mathbf{Q}, \mathbf{Q}')}{\partial q'_1} & \frac{\partial K(\mathbf{Q}, \mathbf{Q}')}{\partial q'_2} & \dots & \frac{\partial K(\mathbf{Q}, \mathbf{Q}')}{\partial q'_D} \\ \frac{\partial K(\mathbf{Q}, \mathbf{Q}')}{\partial q_1} & \frac{\partial^2 K(\mathbf{Q}, \mathbf{Q}')}{\partial q_1 \partial q'_1} & \frac{\partial^2 K(\mathbf{Q}, \mathbf{Q}')}{\partial q_1 \partial q'_2} & \dots & \frac{\partial^2 K(\mathbf{Q}, \mathbf{Q}')}{\partial q_1 \partial q'_D} \\ \frac{\partial K(\mathbf{Q}, \mathbf{Q}')}{\partial q_2} & \frac{\partial^2 K(\mathbf{Q}, \mathbf{Q}')}{\partial q_2 \partial q'_1} & \frac{\partial^2 K(\mathbf{Q}, \mathbf{Q}')}{\partial q_2 \partial q'_2} & \dots & \frac{\partial^2 K(\mathbf{Q}, \mathbf{Q}')}{\partial q_2 \partial q'_D} \\ \vdots & \vdots & \vdots & \ddots & \vdots \\ \frac{\partial K(\mathbf{Q}, \mathbf{Q}')}{\partial q_D} & \frac{\partial^2 K(\mathbf{Q}, \mathbf{Q}')}{\partial q_D \partial q'_1} & \frac{\partial^2 K(\mathbf{Q}, \mathbf{Q}')}{\partial q_D \partial q'_2} & \dots & \frac{\partial^2 K(\mathbf{Q}, \mathbf{Q}')}{\partial q_D \partial q'_D} \end{bmatrix}. \quad (14)$$

The variance of the posterior distribution for the potential and force at an unknown point in internal coordinates q^* (corresponding to Cartesian coordinates x^*) is

$$\Lambda_{qq}^{\text{pred}} = K_{\text{ext}}(q^*, q^*) - K_{\text{ext}}(q^*, Q) (K_{\text{ext}}(Q, Q) + \Lambda_{QQ})^{-1} K_{\text{ext}}(Q, q^*). \quad (15)$$

The variance of the posterior distribution in Cartesian coordinates can be obtained using the transformation matrix L :³⁴

$$\Lambda_{xx}^{\text{pred}}(x^*) = \begin{pmatrix} \text{Var}(V) & \text{Cov}(V, f_x) \\ \text{Cov}(f_x, V) & \text{Var}(f_x) \end{pmatrix} = L \Lambda_{qq}^{\text{pred}}(q^*) L^T, \quad (16)$$

$$L = \begin{pmatrix} 1 & 0 \\ 0 & B_q^T \end{pmatrix},$$

where $B_q = \frac{dq}{dx}$ is Wilson's B matrix. The force uncertainty at the unknown point x^* can be estimated by the trace of the force variance matrix $\text{Var}(f_x)$:

$$\sigma_{f,x}^{\text{pred}}(x^*) = \sqrt{\text{Tr}(\text{Var}(f_x(x^*)))}. \quad (17)$$

Acknowledgement

This work was supported by the U.S. Department of Energy, Office of Science, Office of Basic Energy Sciences through the Condensed Phase and Interfacial Molecular Science (CPIMS) Program of the Division of Chemical Sciences, Geosciences, and Biosciences under FWP 80818 (C.Z., N.G.) at the Pacific Northwest National Laboratory (PNNL) and DE-SC0023249 (A.N., M.K. at the University of Washington, Seattle). A.G. acknowledges support from Computational Chemical Sciences Center “Chemistry in Solution and at Interfaces” at Princeton University under DE-SC0019394. This work benefited from computational resources provided by EMSL, a DOE Office of Science User Facility sponsored by the Office of Biological and Environmental Research and located at PNNL, the National Energy Research Scientific Computing Center (NERSC), a U.S. Department of Energy Office of Science User Facility operated under Contract No. DE-AC02-05CH11231, and PNNL’s Institutional Computing Program. PNNL is operated by Battelle Memorial Institute for the United States Department of Energy under DOE Contract No. DE-AC05-76RL1830.

References

- (1) Meyer, H.-D.; Manthe, U.; Cederbaum, L. The multi-configurational time-dependent Hartree approach. Chemical Physics Letters **1990**, 165, 73–78.
- (2) Beck, M.; Jäckle, A.; Worth, G.; Meyer, H.-D. The multiconfiguration time-dependent Hartree (MCTDH) method: a highly efficient algorithm for propagating wavepackets. Physics Reports **2000**, 324, 1–105.
- (3) Wang, H.; Thoss, M. Multilayer formulation of the multiconfiguration time-dependent Hartree theory. The Journal of Chemical Physics **2003**, 119, 1289–1299.
- (4) Soley, M. B.; Bergold, P.; Gorodetsky, A. A.; Batista, V. S. Functional tensor-train

- Chebyshev method for multidimensional quantum dynamics simulations. Journal of chemical theory and computation **2021**, 18, 25–36.
- (5) Lyu, N.; Soley, M. B.; Batista, V. S. Tensor-train split-operator KSL (TT-SOKSL) method for quantum dynamics simulations. Journal of Chemical Theory and Computation **2022**, 18, 3327–3346.
- (6) Chapman, S.; Garrett, B. C.; Miller, W. H. Semiclassical transition state theory for nonseparable systems: Application to the collinear H+H₂ reaction. The Journal of Chemical Physics **1975**, 63, 2710–2716.
- (7) Miller, W. H. Semiclassical limit of quantum mechanical transition state theory for nonseparable systems. The Journal of Chemical Physics **1975**, 62, 1899–1906.
- (8) Callan, C. G.; Coleman, S. Fate of the false vacuum. II. First quantum corrections. Phys. Rev. D **1977**, 16, 1762–1768.
- (9) Grabert, H.; Weiss, U. Crossover from Thermal Hopping to Quantum Tunneling. Phys. Rev. Lett. **1984**, 53, 1787–1790.
- (10) Richardson, J. O.; Althorpe, S. C. Ring-polymer molecular dynamics rate-theory in the deep-tunneling regime: Connection with semiclassical instanton theory. The Journal of Chemical Physics **2009**, 131, 214106.
- (11) Kästner, J. Theory and simulation of atom tunneling in chemical reactions. Wiley Interdisciplinary Reviews: Computational Molecular Science **2014**, 4, 158–168.
- (12) Richardson, J. O. Ring-polymer instanton theory. International Reviews in Physical Chemistry **2018**, 37, 171–216.
- (13) Mills, G.; Schenter, G.; Makarov, D.; Jónsson, H. Generalized path integral based quantum transition state theory. Chemical Physics Letters **1997**, 278, 91–96.

- (14) Richardson, J. O. Derivation of instanton rate theory from first principles. The Journal of Chemical Physics **2016**, 144, 114106.
- (15) Wolynes, P. G. Imaginary time path integral Monte Carlo route to rate coefficients for nonadiabatic barrier crossing. The Journal of Chemical Physics **1987**, 87, 6559–6561.
- (16) Wolynes, P. G. Dissipation, tunneling, and adiabaticity criteria for curve crossing problems in the condensed phase. The Journal of Chemical Physics **1987**, 86, 1957–1966.
- (17) Cao, J.; Voth, G. A. A unified framework for quantum activated rate processes. II. The nonadiabatic limit. The Journal of Chemical Physics **1997**, 106, 1769–1779.
- (18) Richardson, J. O.; Bauer, R.; Thoss, M. Semiclassical Green’s functions and an instanton formulation of electron-transfer rates in the nonadiabatic limit. The Journal of Chemical Physics **2015**, 143, 134115.
- (19) Ansari, I. M.; Heller, E. R.; Trenins, G.; Richardson, J. O. Instanton theory for Fermi’s golden rule and beyond. Philosophical Transactions of the Royal Society A: Mathematical, Physical and Engineering Sciences **2022**, 380, 20200378.
- (20) Grabert, H.; Weiss, U. Crossover from Thermal Hopping to Quantum Tunneling. Phys. Rev. Lett. **1984**, 53, 1787–1790.
- (21) Cao, J.; Voth, G. A. A unified framework for quantum activated rate processes. I. General theory. The Journal of Chemical Physics **1996**, 105, 6856–6870.
- (22) Kryvohuz, M. Semiclassical instanton approach to calculation of reaction rate constants in multidimensional chemical systems. The Journal of Chemical Physics **2011**, 134, 114103.
- (23) Kryvohuz, M. On the derivation of semiclassical expressions for quantum reaction rate constants in multidimensional systems. The Journal of Chemical Physics **2013**, 138, 244114.

- (24) McConnell, S.; Kästner, J. Instanton rate constant calculations close to and above the crossover temperature. Journal of Computational Chemistry **2017**, 38, 2570–2580.
- (25) Lawrence, J. E. Semiclassical instanton theory for reaction rates at any temperature: How a rigorous real-time derivation solves the crossover temperature problem. The Journal of Chemical Physics **2024**, 161, 184115.
- (26) Lawrence, J. E. A unified framework for semiclassical reaction rate theory. The Journal of Chemical Physics **2025**, 163, 234119.
- (27) Lawrence, J. E.; Dušek, J.; Richardson, J. O. Perturbatively corrected ring-polymer instanton theory for accurate tunneling splittings. The Journal of Chemical Physics **2023**, 159, 014111.
- (28) Käser, S.; Richardson, J. O.; Meuwly, M. Accurate Tunneling Splittings for Ever-Larger Molecules from Transfer-Learned, CCSD(T) Quality Energy Functions. 2024; <https://arxiv.org/abs/2407.21366>.
- (29) Richardson, J. O. Microcanonical and thermal instanton rate theory for chemical reactions at all temperatures. Faraday Discuss. **2016**, 195, 49–67.
- (30) McConnell, S. R.; Löhle, A.; Kästner, J. Rate constants from instanton theory via a microcanonical approach. The Journal of Chemical Physics **2017**, 146, 074105.
- (31) Fang, W.; Winter, P.; Richardson, J. O. Microcanonical Tunneling Rates from Density-of-States Instanton Theory. Journal of Chemical Theory and Computation **2021**, 17, 40–55, PMID: 33351621.
- (32) Laude, G.; Calderini, D.; Tew, D. P.; Richardson, J. O. Ab initio instanton rate theory made efficient using Gaussian process regression. Faraday Discuss. **2018**, 212, 237–258.

- (33) Laude, G.; Calderini, D.; Welsch, R.; Richardson, J. O. Calculations of quantum tunnelling rates for muonium reactions with methane, ethane and propane. Phys. Chem. Chem. Phys. **2020**, 22, 16843–16854.
- (34) Fang, W.; Zhu, Y.-C.; Cheng, Y.; Hao, Y.-P.; Richardson, J. O. Robust Gaussian Process Regression Method for Efficient Tunneling Pathway Optimization: Application to Surface Processes. Journal of Chemical Theory and Computation **2024**, 20, 3766–3778, PMID: 38708859.
- (35) Cooper, A. M.; Hallmen, P. P.; Kästner, J. Potential energy surface interpolation with neural networks for instanton rate calculations. The Journal of Chemical Physics **2018**, 148, 094106.
- (36) Einarsdóttir, D. M.; Arnaldsson, A.; Óskarsson, F.; Jónsson, H. Path optimization with application to tunneling. Applied Parallel and Scientific Computing: 10th International Conference, PARA 2010, Reykjavík, Iceland, June 6-9, 2010, Revised Selected Papers, Part II 10. 2012; pp 45–55.
- (37) Ásgeirsson, V.; Arnaldsson, A.; Jónsson, H. Efficient evaluation of atom tunneling combined with electronic structure calculations. The Journal of Chemical Physics **2018**, 148, 102334.
- (38) Henkelman, G.; Uberuaga, B. P.; Jónsson, H. A climbing image nudged elastic band method for finding saddle points and minimum energy paths. The Journal of Chemical Physics **2000**, 113, 9901–9904.
- (39) Henkelman, G.; Jónsson, H. Improved tangent estimate in the nudged elastic band method for finding minimum energy paths and saddle points. The Journal of Chemical Physics **2000**, 113, 9978–9985.
- (40) Zhang, C.; Nimmrich, A.; Johnson, B. A.; Schenter, G. K.; Khalil, M.; Govind, N. Accelerating Instanton Theory with the Line Integral Nudged Elastic Band Method

- and Gaussian Process Regression. Journal of Chemical Theory and Computation **2025**, 21, 7517–7534, PMID: 40674652.
- (41) Cvitaš, M. T.; Althorpe, S. C. Locating Instantons in Calculations of Tunneling Splittings: The Test Case of Malonaldehyde. Journal of Chemical Theory and Computation **2016**, 12, 787–803, PMID: 26756608.
- (42) Cvitaš, M. T. Quadratic String Method for Locating Instantons in Tunneling Splitting Calculations. Journal of Chemical Theory and Computation **2018**, 14, 1487–1500, PMID: 29360359.
- (43) E, W.; Ren, W.; Vanden-Eijnden, E. String method for the study of rare events. Phys. Rev. B **2002**, 66, 052301.
- (44) E, W.; Ren, W.; Vanden-Eijnden, E. Simplified and improved string method for computing the minimum energy paths in barrier-crossing events. The Journal of Chemical Physics **2007**, 126, 164103.
- (45) Garrido Torres, J. A.; Jennings, P. C.; Hansen, M. H.; Boes, J. R.; Bligaard, T. Low-Scaling Algorithm for Nudged Elastic Band Calculations Using a Surrogate Machine Learning Model. Phys. Rev. Lett. **2019**, 122, 156001.
- (46) Meyer, R.; Hauser, A. W. Geometry optimization using Gaussian process regression in internal coordinate systems. The Journal of Chemical Physics **2020**, 152, 084112.
- (47) Born, D.; Kästner, J. Geometry Optimization in Internal Coordinates Based on Gaussian Process Regression: Comparison of Two Approaches. Journal of Chemical Theory and Computation **2021**, 17, 5955–5967, PMID: 34378918.
- (48) Gardner, J.; Pleiss, G.; Weinberger, K. Q.; Bindel, D.; Wilson, A. G. Gpytorch: Black-box matrix-matrix gaussian process inference with gpu acceleration. Advances in neural information processing systems **2018**, 31.

- (49) Beyer, A. N.; Richardson, J. O.; Knowles, P. J.; Rommel, J.; Althorpe, S. C. Quantum Tunneling Rates of Gas-Phase Reactions from On-the-Fly Instanton Calculations. The Journal of Physical Chemistry Letters **2016**, 7, 4374–4379, PMID: 27775889.
- (50) Bitzek, E.; Koskinen, P.; Gähler, F.; Moseler, M.; Gumbusch, P. Structural Relaxation Made Simple. Phys. Rev. Lett. **2006**, 97, 170201.
- (51) Guérolé, J.; Nöhling, W. G.; Vaid, A.; Houllé, F.; Xie, Z.; Prakash, A.; Bitzek, E. Assessment and optimization of the fast inertial relaxation engine (fire) for energy minimization in atomistic simulations and its implementation in lammmps. Computational Materials Science **2020**, 175, 109584.
- (52) Sheppard, D.; Terrell, R.; Henkelman, G. Optimization methods for finding minimum energy paths. The Journal of Chemical Physics **2008**, 128, 134106.
- (53) Witkin, A. Physically based modeling: principles and practice constrained dynamics. Computer graphics **1997**, 9, 27.
- (54) Koistinen, O.-P.; Ásgeirsson, V.; Vehtari, A.; Jónsson, H. Minimum Mode Saddle Point Searches Using Gaussian Process Regression with Inverse-Distance Covariance Function. Journal of Chemical Theory and Computation **2020**, 16, 499–509, PMID: 31801018.
- (55) Denzel, A.; Kästner, J. Hessian Matrix Update Scheme for Transition State Search Based on Gaussian Process Regression. Journal of Chemical Theory and Computation **2020**, 16, 5083–5089, PMID: 32609514.
- (56) Koistinen, O.-P.; Maras, E.; Vehtari, A.; Jónsson, H. Minimum energy path calculations with Gaussian process regression. Nanosystems: Physics, Chemistry, Mathematics **2016**, 925–935.

- (57) Koistinen, O.-P.; Ásgeirsson, V.; Vehtari, A.; Jónsson, H. Nudged Elastic Band Calculations Accelerated with Gaussian Process Regression Based on Inverse Interatomic Distances. Journal of Chemical Theory and Computation **2019**, 15, 6738–6751, PMID: 31638795.
- (58) Gardner, J. R.; Pleiss, G.; Bindel, D.; Weinberger, K. Q.; Wilson, A. G. GPyTorch: Blackbox Matrix-Matrix Gaussian Process Inference with GPU Acceleration. *Advances in Neural Information Processing Systems*. 2018.
- (59) Nocedal, J.; Wright, S. J. Numerical optimization; Springer, 1999.
- (60) Hutchinson, M. A stochastic estimator of the trace of the influence matrix for laplacian smoothing splines. Communications in Statistics - Simulation and Computation **1990**, 19, 433–450.
- (61) Meyer, R. A.; Musco, C.; Musco, C.; Woodruff, D. P. Hutch++: Optimal Stochastic Trace Estimation. 2021; <https://arxiv.org/abs/2010.09649>.
- (62) Litman, Y.; Richardson, J. O.; Kumagai, T.; Rossi, M. Elucidating the Nuclear Quantum Dynamics of Intramolecular Double Hydrogen Transfer in Porphycene. Journal of the American Chemical Society **2019**, 141, 2526–2534, PMID: 30648386.
- (63) Mil'nikov, G. V.; Nakamura, H. Practical implementation of the instanton theory for the ground-state tunneling splitting. The Journal of Chemical Physics **2001**, 115, 6881–6897.
- (64) Richardson, J. O.; Althorpe, S. C. Ring-polymer instanton method for calculating tunneling splittings. The Journal of Chemical Physics **2011**, 134, 054109.
- (65) Kawatsu, T.; Miura, S. Efficient algorithms for semiclassical instanton calculations based on discretized path integrals. The Journal of Chemical Physics **2014**, 141, 024101.

- (66) Richardson, J. O. Full- and reduced-dimensionality instanton calculations of the tunnelling splitting in the formic acid dimer. Phys. Chem. Chem. Phys. **2017**, 19, 966–970.
- (67) Qu, C.; Bowman, J. M. An ab initio potential energy surface for the formic acid dimer: zero-point energy, selected anharmonic fundamental energies, and ground-state tunneling splitting calculated in relaxed 1–4-mode subspaces. Phys. Chem. Chem. Phys. **2016**, 18, 24835–24840.
- (68) Ortlieb, M.; Havenith, M. Proton Transfer in (HCOOH)₂: An IR High-Resolution Spectroscopic Study of the Antisymmetric C-O Stretch. The Journal of Physical Chemistry A **2007**, 111, 7355–7363, PMID: 17552500.
- (69) Goroya, K. G.; Zhu, Y.; Sun, P.; Duan, C. High resolution jet-cooled infrared absorption spectra of the formic acid dimer: A reinvestigation of the C–O stretch region. The Journal of Chemical Physics **2014**, 140, 164311.
- (70) Zhang, Y.; Liu, Z.; Yang, Y. Finite-Temperature Double Proton Transfer in Formic Acid Dimer via Constrained Nuclear-Electronic Orbital Molecular Dynamics: Lower Barriers and Enhanced Rates from Nuclear Quantum Delocalization. Journal of Chemical Theory and Computation **2025**, 21, 5400–5408, PMID: 40405364.
- (71) Karney, C. F. Quaternions in molecular modeling. Journal of Molecular Graphics and Modelling **2007**, 25, 595–604.
- (72) Behler, J. Atom-centered symmetry functions for constructing high-dimensional neural network potentials. Journal of Chemical Physics **2011**, 134, Cited by: 1269.
- (73) Bartók, A. P.; Kondor, R.; Csányi, G. On representing chemical environments. Phys. Rev. B **2013**, 87, 184115.
- (74) Li, F.; Yang, X.; Liu, X.; Cao, J.; Bian, W. An Ab Initio Neural Network Potential En-

- ergy Surface for the Dimer of Formic Acid and Further Quantum Tunneling Dynamics. ACS Omega **2023**, 8, 17296–17303.
- (75) Zhang, Y.; Li, W.; Luo, W.; Zhu, Y.; Duan, C. High resolution jet-cooled infrared absorption spectra of (HCOOH)₂, (HCOOD)₂, and HCOOH-HCOOD complexes in 7.2 μm region. The Journal of Chemical Physics **2017**, 146, 244306.
- (76) Li, W.; Evangelisti, L.; Gou, Q.; Caminati, W.; Meyer, R. The Barrier to Proton Transfer in the Dimer of Formic Acid: A Pure Rotational Study. Angewandte Chemie International Edition **2019**, 58, 859–865.
- (77) Firth, D. W.; Beyer, K.; Dvorak, M. A.; Reeve, S. W.; Grushow, A.; Leopold, K. R. Tunable far-infrared spectroscopy of malonaldehyde. The Journal of Chemical Physics **1991**, 94, 1812–1819.
- (78) Baba, T.; Tanaka, T.; Morino, I.; Yamada, K. M. T.; Tanaka, K. Detection of the tunneling-rotation transitions of malonaldehyde in the submillimeter-wave region. The Journal of Chemical Physics **1999**, 110, 4131–4133.
- (79) Sewell, T. D.; Guo, Y.; Thompson, D. L. Semiclassical calculations of tunneling splitting in malonaldehyde. The Journal of Chemical Physics **1995**, 103, 8557–8565.
- (80) Käser, S.; Richardson, J. O.; Meuwly, M. Transfer Learning for Affordable and High-Quality Tunneling Splittings from Instanton Calculations. Journal of Chemical Theory and Computation **2022**, 18, 6840–6850, PMID: 36279109.
- (81) Zhang, J.; Zhang, H.; Ye, H.; Zheng, Y. Free-end adaptive nudged elastic band method for locating transition states in minimum energy path calculation. The Journal of Chemical Physics **2016**, 145, 094104.